Paired longitudinal live-cell imaging and transcriptomics enable deeper characterization of cells

Pier Federico Gherardini[1], Mehdi Mohseni[1], Saege Hancock[1], Brandon Razooky[1], Shan Sabri[1], Richard Yau[1], Sophia Espanola[1], Nirvan Rouzbeh[1], Olaia Villa[1], Marc Laurent[1], Gary Schroth[1]

[1]Cellanome, Foster City, CA, USA

The relationship between gene expression and cellular function is complex: transcriptomic measurements provide static snapshots, while cellular phenotypes unfold over time. To bridge this gap, we developed CellCage™ Technology, which leverages light-guided hydrogel polymerization to enable longitudinal imaging of individual cells coupled with endpoint transcriptomics. Within this system, imaging provides unambiguous readouts of complex cellular functions linked to underlying transcriptional programs. To characterize information-rich imaging phenotypes, we leveraged DINOv2, a self-supervised vision transformer, to extract high-dimensional morphological features with dimensionality comparable to gene expression. This combination of imaging and transcriptomics represents a novel paired datatype that reveals biological insights inaccessible to transcriptomics alone. To further leverage the imaging data, we developed a live cell painting panel and demonstrated that it enables better cell type prediction from morphological features. In preadipocytes and microglia, paired data uncovered functional driver genes that transcriptomic clustering alone failed to identify.

Cellanome R3200: A Platform Integrating Longitudinal Live Cell Imaging With Transcriptomics

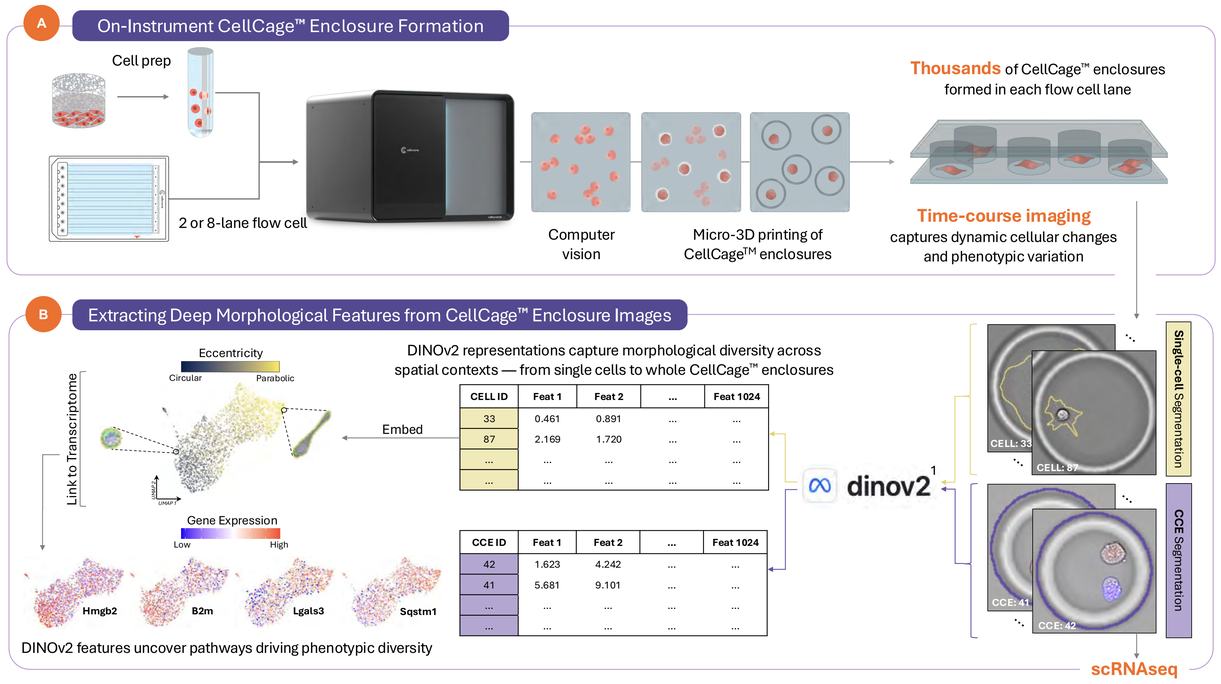


Fig. 1. Integrated experimental and computational workflow linking morphology and transcriptomics. A: Schematic of Cellanome's CellCage™ technology, which enables multi-modal phenotypic and functional profiling of the same live cells. Tens of thousands of cells are mixed with a hydrogel precursor and loaded into a multi-lane flow cell. Individual cells are located, and CellCage™ enclosures (CCEs) are automatically generated around them via light-guided polymerization. The CCEs are permeable to small molecules and antibodies, allowing long-term culture and time-course imaging of the same cells. Following imaging-based assays, cells are lysed *in situ*, and mRNA is captured for cDNA synthesis, library preparation, and sequencing on an external instrument. **B:** DINOv2-based computational workflow for extracting high-dimensional morphological embeddings from CCE images. These features capture phenotypic variation across scales — from single cells to entire CCEs — and can be integrated with single-cell transcriptomic data to reveal morphology–gene expression relationships.

DINOv2: A Self-Supervised Model for Extracting Morphological Features from Images

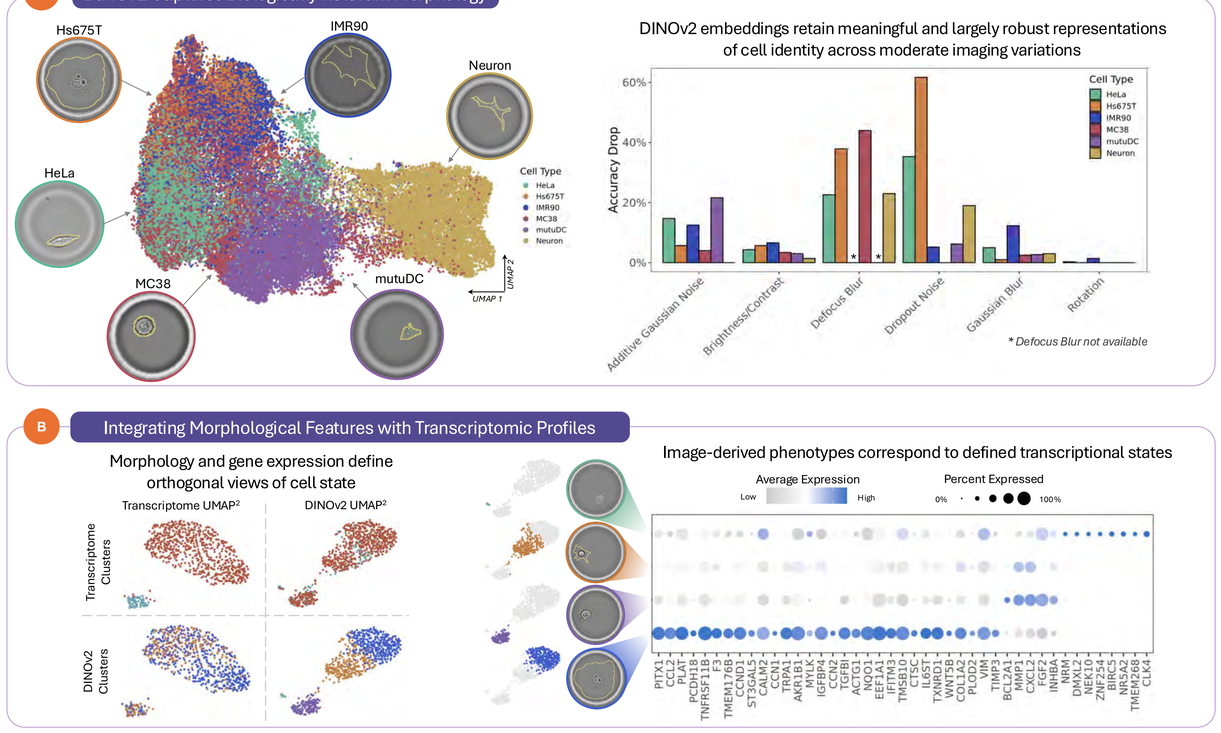


Fig. 2. Validation of DINOv2 morphological embeddings. A: DINOv2 features from six cell lines clustered by cell identity, confirming capture of meaningful morphological differences. Embedding similarity predicted the generalization performance of a Mask R-CNN (Region-based Convolutional Neural Network) segmentation model. The embeddings remained robust under common image augmentations, supporting their use for integration with transcriptomic data. **B:** Clustering of DINOv2 features from fibroblast CCE images identified four distinct morphological states — ranging from fully adhered, ECM-enriched cells (CCN2, ST3GAL5; Blue cluster) to weakly adhered, inflammatory cells (CXCL2, MMP1; Orange cluster), with intermediate adhesion–stress profiles. These morphology-defined phenotypes were undetectable by transcriptomic clustering alone, demonstrating that image-derived embeddings capture functionally relevant cellular heterogeneity.

Live Cell Painting Predicts Cell Identity As Defined By Paired Transcriptomic Data

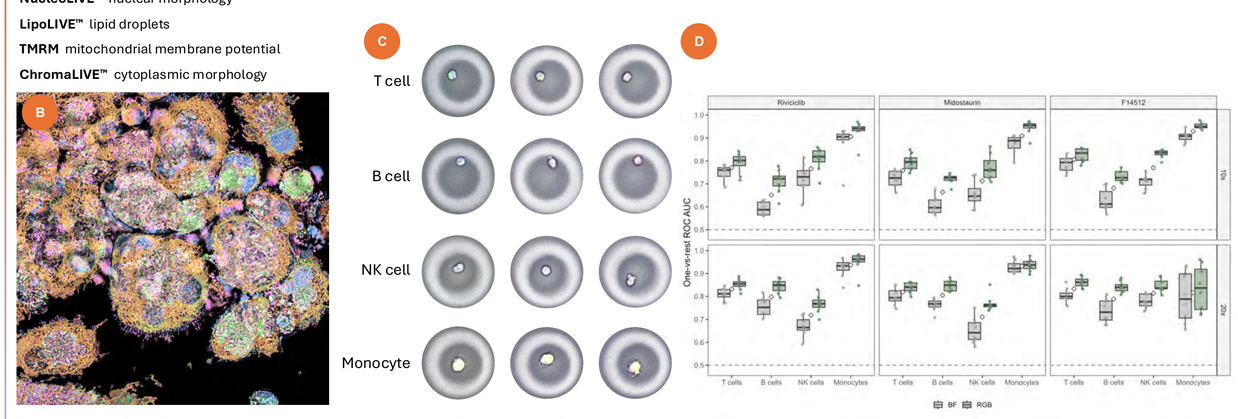


Fig. 3. Live Cell Painting predicts cell identity in Peripheral Blood Mononuclear Cells. A: We developed a Live Cell Painting (LCP) panel for longitudinal live cell imaging using the Saguaro dyes NucleoLIVE, LipoLIVE and ChromaLive combined with TMRM. **B**: Representative image of U2OS cells stained with the LCP panel and imaged using a 60x oil immersion objective in a cell culture plate. **C**: Representative longitudinal images of different cell populations (as identified by transcriptomics) from Peripheral Blood Mononuclear Cells compartmentalized in CCEs. The images are in brightfield with overlaid fluorescence channels for the LCP panel at 20x magnification. **D:** We evaluated the ability of DINOv2 embeddings calculated from brightfield-only or brightfield + LCP images to predict cell type identity as defined by paired transcriptomic data from the same cells. Each plot facet correspond to one of six separate experiments (columns: 3 drug treatments, rows: 2 magnifications). Each experiments comprises 8 lanes of a single flow cell, corresponding to different drug dosages and stimulation conditions. For each lane we trained a separate ElasticNet classifier to distinguish each cell population (as defined by the paired transcriptomic data) vs the rest, using as input the DINOv2 embeddings for each cell image. The boxplots show the average Area Under the Curve (AUC) across the different flow cell lanes of the various classifiers for each cell type when using brightfield images (gray boxes) vs brightfield + LCP images (green boxes). For most experiments, including the LCP information improves the accuracy of cell type prediction.

Longitudinal Imaging Combined With Transcriptomics Identifies Drivers of Preadipocytes Differentiation

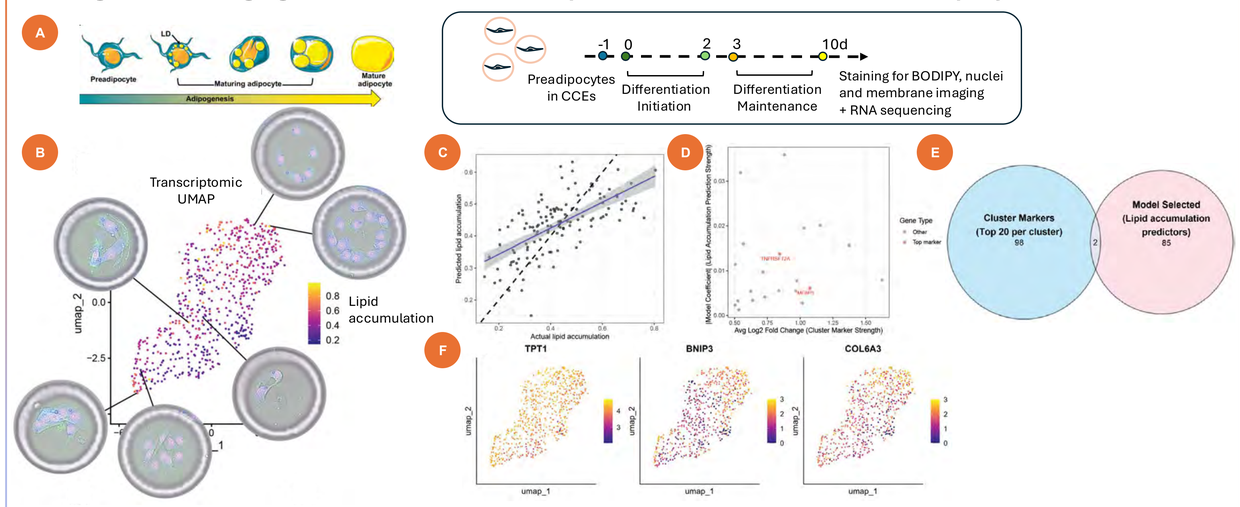


Fig. 4. Characterizing preadipocyte differentiation on a Cellanome flow cell. A: Diagram of the experimental workflow. **B**: Lipid accumulation score (ratio of BODIPY to nuclear signal) does not segregate with global transcriptomic patterns. **C:** ElasticNet prediction of lipid accumulation scores from gene expression data. The x and y axis correspond to the actual and predicted values respectively. **D**: Average Log2 fold-change between clusters (x axis) vs absolute model coefficient (y axis) for the genes selected by the model. Red genes are among the top-20 differentially expressed genes between transcriptomic clusters. **E**: Overlap between top-20 differentially expressed genes between transcriptomic clusters (blue) and model-selected predictors of lipid accumulation (pink). **F**: Expression UMAP colored by the top-3 positive model predictors, showing that the expression values of these genes are uniformly distributed

A Functional Assay To Identify Genes Associated With Phagocytic Activity

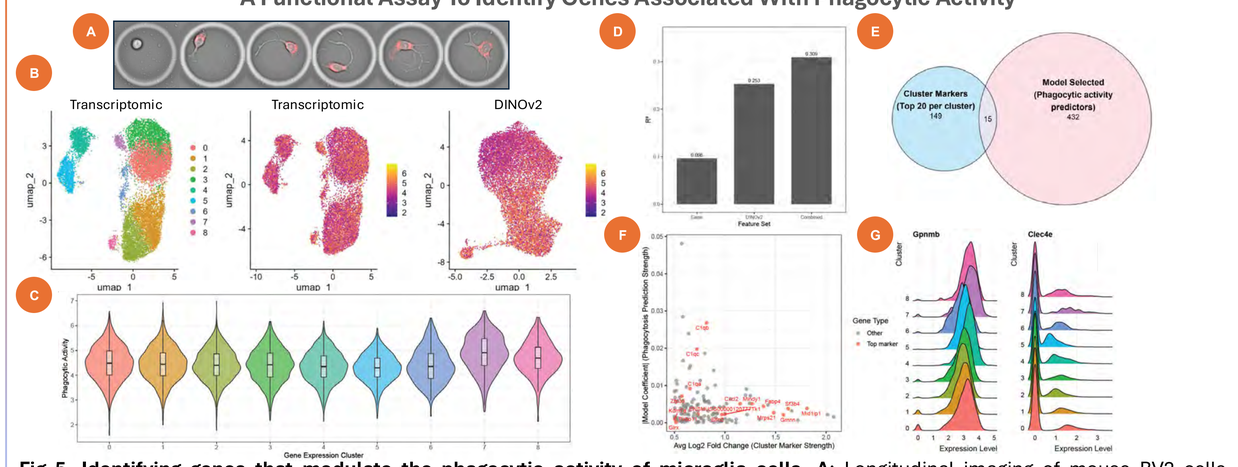


Fig 5. Identifying genes that modulate the phagocytic activity of microglia cells. A: Longitudinal imaging of mouse BV2 cells phagocytosing pHrodo particles. **B:** UMAPs based on the gene expression data (left and center), show that phagocytic activity is uniformly distributed. The UMAP based on the DINOv2 features (right) shows better correlation. **C**: Distribution of phagocytic activity across expression-derived clusters. **D**: R^2 performance of different ElasticNet models trained to predict phagocytic activity. **E**: Minimal overlap between top-20 differentially expressed genes between transcriptomic clusters and model-selected predictors of phagocytic activity. **F**: Average Log2 fold-change between clusters (x axis) vs absolute model coefficients (y axis) for the genes selected by the expression-only model. Red genes are among the top-20 differentially expressed genes between transcriptomic clusters. **G**: Gpnmb and Clec4e are among the top positive predictors for the gene expression-based model and have clear mechanistic evidence linking them to the phagocytosis process. However, their expression is very similar across all the transcriptomic clusters.

COPYRIGHT CELLANOME 2026 | Cellanome, Foster City, CA USA